Structure of Bacterial Extracellular Polymeric Substances at Different pH Values as Determined by SAXS

Iztok Dogsa,*† Manfred Kriechbaum,‡ David Stopar,† and Peter Laggner‡

*Laboratory for Biophysics, Jozef Stefan Institute, Ljubljana, Slovenia; †Biotechnical Faculty, Department of Food Technology, Laboratory of Microbiology, University of Ljubljana, Ljubljana, Slovenia; and ‡Institute of Biophysics and X-Ray Structure Research, Graz, Austria

ABSTRACT   Extracellular polymeric substances (EPS) play an important role in cell aggregation, cell adhesion, and biofilm formation, and protect cells from a hostile environment. The EPS was isolated by trichloroacetic acid/ethanol extraction from broth culture of a marine bacterium isolate. The EPS was composed of glucose and galactose as determined by HPLC and TLC; the protein content was on average $15 \pm 5\%$ of EPS dry mass. The solution structure of EPS at different values of pH was revealed by small-angle x-ray scattering. Scattering curves of EPS solutions (0.4%, w/v) consistently showed two nearly linear log-log regions with slopes a and b in the q-ranges from 0.06 nm^{-1} to 0.26 nm^{-1}, and from 0.27 nm^{-1} to 0.88 nm^{-1}, respectively. Slope a was sensitive to pH changes whereas slope b was not. The observed sensitivity to pH was not a consequence of ionic strength variation with pH, as checked by salt addition. The pH variation causes major rearrangements of EPS structure mainly at length scales above 24 nm. To get a better understanding of the pH effect on EPS structure, the original model proposed by Geissler was refined into a mathematical model that enabled fitting of the experimental scattering curves in the pH range from 0.7 to 11.0. The model describes EPS structure as a network of randomly coiled polymeric chains with denser domains of polymeric chains. The results obtained from the model indicate that dense domains increase in average size from 19 nm at pH 11.0 to 52 nm at pH 0.7. The average distance between the polysaccharide chains at pH 0.7 was 2.3 nm, which indicates a compact EPS structure. Swelling was found to be at a maximum around pH = 8.8, where the average distance between the chains was 4.8 nm.

INTRODUCTION

The major component of the microbial extracellular polymeric substances (EPS) would be the extracellular polysaccharides, which are associated either with the cell surface or excreted in the growth medium (1). In the isolated extracellular polymeric substances, proteins may be recovered as well (2–6). The EPS plays an important role in cell aggregation (7), cell adhesion (8,9), biofilm formation (10,11), and protection of cells from hostile environments (10,12). The extracellular polysaccharides secreted in the media by industrial microorganisms improve the quality of the product (13,14). On the other hand, extracellular polymeric substances in biofilms cause hygienic problems in the food industry (15). Adherent bacterial communities embedded in a polysaccharide matrix cause persistent human infections that are highly resistant to antibiotics (16). Microbial activity in biofilms can cause material deterioration and economic loss (17,18).

Many of the EPS physicochemical properties are closely linked to the three-dimensional structure of the biopolymer network. EPS structures have been studied on different model systems and by applying different spectroscopic techniques. Larger network structures with regions of unequal densities were visualized by electron microscopy in hyaluronan from *Streptococcus equi* (19). Fibrous structures were seen by scanning electron microscopy in EPS from *Bacillus* sp. (20). Double helices were observed in rhamsan after deacetylation by optical rotation spectroscopy and dif-

ferential scanning calorimetry (21). Similar results were obtained by atomic force microscopy in a combination with static light scattering on extracellular polysaccharides from *Acetobacter xylinim* (22). From rheological studies, it follows that EPS of *Erwinia chrysanthemi* spp. forms elastic coiled structures (23).

Small-angle x-ray scattering (SAXS) techniques have also been frequently used in studying polysaccharide structures. For example, SAXS measurements indicated that cross-linked hyaluronan consists of randomly distributed zones of denser material (19). In a related work, Hirata et al. (24) has considered dextran solutions from several bacterial genera as networks with embedded static heterogeneous domains of higher polymer concentration. Temperature transitions of gellan, carrageenan, and curdlan have been investigated by SAXS. The impact of inorganic salts on carrageenan and gellan gelation mechanism has also been studied by SAXS (25–27). Little is known, however, on the effect of pH on EPS structure. For instance, rheological studies by Yang et al. (28) have shown that curdlan structure appears to be pH-dependent, i.e., it forms random coils at neutral pH, and rodlike structures at high pH (29).

In this article, we report on SAXS studies of the structure of EPS from recently isolated marine bacterium from the Northern Adriatic Sea, where mucilage formation that causes severe economic loss is frequently reported. The work was aimed at an elucidation of the structural effects of pH on EPS structure and the results allow new insight into the swelling behavior of this network-gel. From a technical point of view, the results demonstrate that detailed information on dilute,

low-contrast systems can be obtained from x-ray scattering with suitable laboratory instruments even without the use of synchrotron radiation.

MATERIALS AND METHODS

Bacterial growth

Slime-producing marine bacterial isolate, recently isolated from the Northern Adriatic Sea, was used for the purpose of this study. The isolate was morphologically characterized as pleomorphic rod. According to the physiological tests, the isolate is: G −; Oxidase +; Catalase +; it has no pigment; OF glucose O+F−; Gelatinase +; Cellulase −; Lipase −; Lecithinase −; motile; able to grow at 4°C; unable to grow at 42°C; unable to grow anaerobically; and unable to grow without NaCl. Based on this test we were not able to relate it to the known bacterial species. The bacterial isolate was grown in PYE medium (0.1 g yeast extract, 0.5 g peptone, 0.2 g MgCl$_2$, and 1.76 g NaCl in 100 ml of deionized water). Fresh medium was inoculated with 2% overnight bacterial culture and incubated on a rotary shaker (250 rpm) for 24 h at 27°C.

EPS isolation and sample preparation

Purely native bacterial polysaccharides are difficult to study, since most polysaccharide matrices contain significant amounts of other substances (e.g., proteins, nucleic acids, lipids). In addition, the concentration of polysaccharides in the bacterial culture is usually too low to study directly. Therefore, the polysaccharides were purified and concentrated according to the modified method of Faber et al. (30). Typically, proteins in the supernatant were precipitated by addition of trichloroacetic acid to a final concentration of 8% (w/v). The mixture was stirred for 45 min and the cell debris was removed by centrifugation (5000 rpm, 1 h). The EPS in the supernatant was precipitated by addition of 2 volumes of cold ethanol (96%), and left overnight at 4°C. The collected precipitate was dialyzed against a 100-fold excess of distilled water. The distilled water was changed three times every 24 h. Even after extensive dialysis against water, some divalent ions might still have been present in our sample. However, in terms of preserving the native polysaccharide structure, removal of divalent ions might have caused some perturbation and was therefore avoided. After dialysis, the EPS was recovered by addition of 2 volumes of ethanol (96%). The precipitate was collected and dried on a rotary evaporator. Dried EPS was stored at 4°C before SAXS analyses. The EPS yields were from 40- to 60-mg dry weight per liter of growth medium.

For SAXS measurements, dry EPS was dissolved in a buffer solution to obtain the desired pH. Final concentration of the EPS was 0.4% (w/v). For pH measurements the stock solutions of 0.2 M citric acid, 0.4 M Na$_2$HPO$_4$, 0.2 M Na$_2$CO$_3$, and 0.2 M solution of H$_3$BO$_3$ with 0.2 M KCl were prepared. The acidic buffers (pH from 2.5 to 7.0) were then obtained by mixing 0.2 M citric acid with 0.4 M Na$_2$HPO$_4$ at different volume ratios so that the final volume was kept constant. The alkaline buffers (pH from 8.0 to 11.0) were obtained by mixing 0.2 M Na$_2$CO$_3$ with 0.2 M solution of H$_3$BO$_3$ with 0.2 M KCl at different volume ratios so that the final volume was again kept constant. For pH 0.7, 0.2 M HCl was used. Each sample was separately prepared by dissolving the dry EPS in the buffer with appropriate pH. The samples were incubated for 1 h before the SAXS measurements. To check whether irreversible chemical modifications such as hydrolysis may have occurred at low pH, the EPS was exposed to 1 M HCl for 8 h. The hydrolysis was additionally studied by heating the EPS sample for 1 h in 1 M HCl at 100°C. The SAXS measurements were taken at room temperature. To see if the SAXS scattering curve is affected by increased concentration of EPS, we prepared either 0.4 or 1% (w/v) EPS water solutions. The effect of ionic strength on SAXS scattering curves was checked in 0.4% (w/v) EPS water solutions, with NaCl or CaCl$_2$ added to the same sample to the final concentrations of 0.5, 1.0, and 2.0 M. The SAXS scattering curves were reproducible.

Chemical composition of EPS

For determination of monosaccharide composition with TLC and HPLC, the samples were hydrolyzed at 100°C for 4 h in 6 M HCl. The TLC analysis was done as described by Pukl and Prosek (31). Silica gel 60F$_{254}$ HPTLC plates, pre-washed by running a blank chromatogram in a mixture of methanol-water (9:1, v/v) and activated at 120°C for 20 min, were used. A standard mixture contained glucose, fructose, mannose, and galactose. Separation was carried out in normal, unsaturated chambers at room temperature (23°C), using an acetonitrile-water (85:15, v/v) solvent system. The dried plates were dipped into aniline-diphenylamine reagent. After heating to 120°C for 10 min, colored spots of sugars appeared. The HPLC system used consisted of a Maxi Star K-1000 pump (Knauer, Berlin, Germany), a K-2301 RI detector (Knauer), and a Luna 5-μm NH2 column (Phenomenex, Torrance, CA); the injection valve was fitted with a 20-μl injection loop and the samples were introduced to the valve via a Marathon-XT autosampler (Spark Holland, Emmen, The Netherlands). Mobile phase was bi-distilled water, operational temperature and flow rate were 85°C and 0.6 mL/min, respectively. A standard mixture contained glucose, fructose and galactose. Protein content of crude EPS was analyzed using a Bio-Rad protein assay (Bio-Rad Laboratories, Munich, Germany), which is essentially a Bradford assay. The dry EPS was dissolved in hot water. Final concentration of the EPS in samples was 0.1 mg/ml. The light absorption measurements were taken 5 min after addition of Bio-Rad reagent and verified after 1 h on a Lambda-17 UV-VIS spectrometer (Perkin-Elmer, Boston, MA). Bovine serum albumin was used as a protein standard.

Small-angle x-ray scattering

A thin-walled 1-mm-diameter quartz capillary held in a steel cuvette holder was filled with the sample solutions. SAXS experiments were performed on a Hecus SWAXS camera (Hecus X-Ray Systems, Graz, Austria; see also work of Laggner and Mio (32)), using Ni-filtered CuKα-radiation (λ = 1.542 Å) from an RU-200 rotating-anode (Rigaku-Denki, Tokyo, Japan) operating at a power of 4 kW (50 kV, 80 mA). Sample-to-detector distance was 27.8 cm. A linear-position-sensitive detector was used with 1024-channel resolution. Distance between channels was 54 μm. All samples were measured for 1 h at room temperature.

Data analysis

Appropriate pH buffer backgrounds were measured and subtracted from scattering intensities of sample containing EPS. No tail normalization was necessary since wide-angle measurements showed only 0.5% difference in scattering intensity between that of pure water and 0.4% (w/v) EPS. Estimates for scattering length densities, ρ, were calculated by using the online scattering-length calculator on the Internet (33). For this purpose, EPS was assumed to have the net composition of glucose residues, and a mass density of 1.3 g/cm^3. The calculated ρ for EPS was comparable with the estimate for carrageenan (34). Buffer mass densities were estimated under the assumption that after addition of salts, only the mass of solution changes, whereas the volume of solution remains constant. For HCl solutions, the values for mass densities were obtained from the work of Trpinac (35). Experimental data were fitted with Eq. 4 using computer software Origin 6.1 Pro (OriginLab Corporation, Northampton, MA). The nonlinear model and the Levenberg-Marquardt method were chosen. The criteria for goodness of fit were: 1), reduced χ-squared test divided by degrees of freedom; and 2), visual quality of the fit on all types of graphical presentations (i.e., linear, log-log, and Kratky-Porod plot).

RESULTS

Both HPLC and TLC analyses of isolated and hydrolyzed polysaccharides detected two monosaccharide sugars,

glucose and galactose, in the EPS. The fraction of galactose did not exceed 10%. In addition, proteins have been detected in the isolated EPS. The protein content of EPS was, on average, $15 \pm 5\%$ of EPS dry mass. The isolated EPS was investigated by SAXS. A representative experimental, slit-smeared SAXS scattering curve intensity $I(q)$ of 0.4% (w/v) EPS, plotted as a function of absolute value of scattering vector $q = 4\pi \sin \theta/\lambda$ (where 2θ is scattering angle, and λ is wavelength), is shown in Fig. 1 a. The double-logarithmic plot in Fig. 1 b indicates the presence of two approximately linear regions, with slopes a and b. Slope a was determined in the q-range from 0.06 to 0.26 nm^{-1}, and slope b from 0.27 to 0.88 nm^{-1}.

The effect of different pH values on slopes a and b is given in Fig. 2. When dry EPS was dissolved at different pH values, samples dissolved better at alkaline pH than at acidic pH. The majority of the material was nevertheless dispersed in the capillary in a form of macroscopic particles. The SAXS observation scale (up to 100 nm), however, is far below the visible range, and the scattering curve is not directly affected by the macroscopic particles. The two SAXS size-scales present in the EPS structure are influenced by pH to different extents. An increase of the solvent pH resulted in an increase of slope a. The relationship was sigmoidal ($R^2 = 0.95$), with the midpoint around pH 6.5. Slope a changed significantly from -0.8 at pH 11 to -2.4 at pH 0.7. Slope b, on the other hand, did not show any apparent dependence on pH, and the values were scattered in the range from -0.9 to -1.2. The reversibility of the EPS structural changes upon adjusting pH back to the initial value was not studied. Because of a relatively large pH range in the experiment, it is possible that the difference measured in the structure of EPS could be a consequence of a relatively large ionic-strength difference. To determine the significance of pH relative to the ionic strength on the scattering intensity, the EPS samples were treated with NaCl and $CaCl_2$. Slope a increased with increased salt concentration, as given in Table 1. In sharp contrast to the pH effect, slope b increased with increasing salt concentration. If the effect of pH were superimposed on the effect of ionic strength, one would expect a change of the
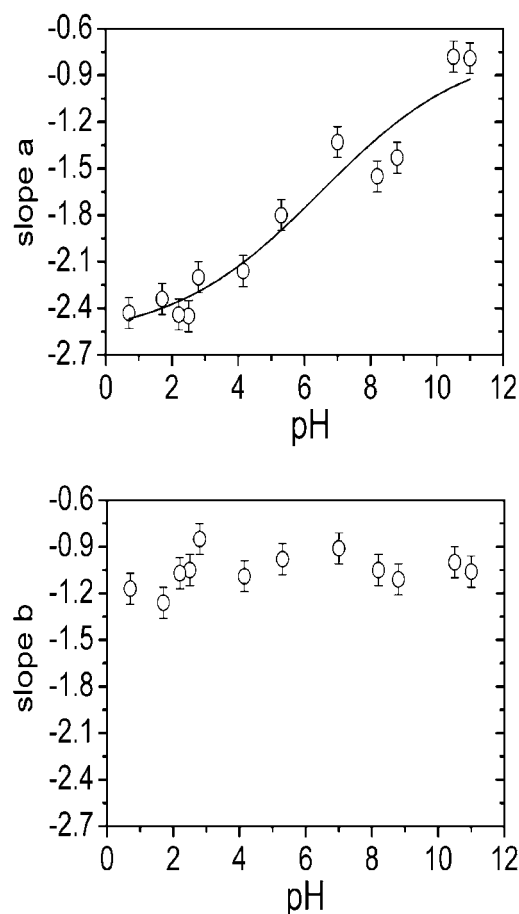

FIGURE 2 The effect of pH on slopes a and b in the scattering curves for 0.4 (w/v) % EPS. The effect is most pronounced on slope a, indicating changes on scales above 24 nm.

slope b with pH. This was not observed. The effect of a divalent $CaCl_2$ on EPS structure was somewhat stronger than for NaCl. The spread of the experimental data for slope a in pH experiments was 1.6 ± 0.3, which was much more than in the experiments where salt concentration was varied (i.e., 0.25 ± 0.2 and -0.1 ± 0.2 for NaCl and $CaCl_2$,
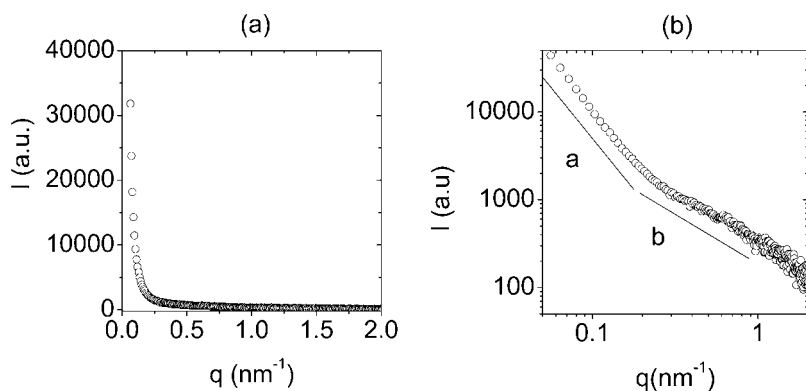

FIGURE 1 SAXS scattering curve $I(q)$ for 0.4% (w/v) EPS in water at room-temperature in linear (a) and double-logarithmic (b) plots. Two nearly linear regions with slopes a and b are indicated, suggesting two characteristic structural length-scales.

TABLE 1 The effect of NaCl and CaCl$_2$ concentration on the slopes _a_ and _b_ obtained from a log-log SAXS scattering curves at pH 4.8

Salt concentration [M]	I_s NaCl [M]	I_s CaCl$_2$ [M]	NaCl	CaCl$_2$
				Slope _a_
0.0	0	0	−1.85	−1.75
0.5	1.0	1.1	−1.60	−1.75
1.0	2.0	2.1	−1.60	−1.85
2.0	4.0	4.2	−1.50	−1.25
				Slope _b_
0.0	0	0	−1.10	−1.15
0.5	1.0	1.1	−0.95	−0.90
1.0	2.0	2.1	−0.90	−0.80
2.0	4.0	4.2	−0.80	−0.30

I_s denotes calculated ionic strength of the solution. The error estimates for _a_ and _b_ are ±0.1.

respectively). This indicates that proton concentration had stronger effect on EPS structure, compared to the ionic strength. When 0.4% (w/v) EPS was kept in 1 M HCl for 8 h, no significant change in SAXS scattering curve was observed, compared to the sample that was in 1 M HCl for 1 h (data not shown). However, after heating the samples of 0.4% (w/v) EPS in 1 M HCl at 100°C for 1 h, there was no structural SAXS signal—implying that hydrolysis may have significantly affected the scattering properties of the sample.

To evaluate EPS structural changes upon pH changes quantitatively, the mathematical model was structured as follows. It was assumed that polymers in the EPS form a gel-like polymeric network consisting of mutually interpenetrated coils. The network is neither symmetrical nor entirely homogeneous in terms of local polymer chain density. There are regions with higher density of polymer with an average diameter Ξ (a static correlation length). These denser domains are considered static in comparison to the regions of the network with lower density. The average distance ξ between polymer chains in the lower-density regions is a dynamic correlation length. The mathematical expression for scattering intensity of gels was already successfully applied by Geissler et al. (36), Horkay et al. (37,38), and Hecht et al. (39), including gels formed by extracellular polysaccharide alginate (40), and is given by the expression

$$I(q) = \Delta\rho^2 \left(\frac{kT\varphi^2}{M_{OS}} \frac{1}{1 + q^2\xi^2} + \sum_j \frac{8\pi\langle\delta\varphi^2\rangle_j \Xi_j^3}{\left(1 + q^2\Xi_j^2\right)^2} \right), \quad (1)$$

where $I(q)$ is scattering intensity normalized to scattering volume; T is the absolute temperature of the polymer; k is the Boltzmann constant; φ is the polymer volume fraction; $\langle\delta\varphi^2\rangle_j$ is the mean-square amplitude of polymer volume fraction fluctuations due to the presence of the jth static inhomogeneity (denser domain); Ξ is the static correlation length; ξ is a dynamic correlation length; $\Delta\rho^2$ is the scattering contrast factor; and M_{OS} is the longitudinal osmotic modulus defined by

$$M_{OS} = \varphi\left(\frac{\partial\pi}{\partial\varphi}\right) + \frac{4G}{3}. \quad (2)$$

Here π is the osmotic pressure, and G the osmotic modulus, which was introduced due to elasticity arising from cross-links (36). There are no cross-links in our model, yet the polymeric coils are assumed to at least partially interpenetrate each other, and therefore elasticity is present.

The problem with the Eq. 1, as given above, is that it is valid for an infinitely narrow primary beam with a point-shaped cross-section. In our case, however, slit collimation was used, producing a beam with a very narrow vertical dimension (half-width <175 μm) and a length of ~2 cm. Therefore, the horizontal width may no longer be ignored. A possible way to overcome this problem is to de-smear the data. Although there are several numerical methods to perform slit de-smearing, all of them implicitly incorporate a degree of data-smoothing as a part of their algorithms. Consequently, starting from the same set of experimental data, de-smeared intensity curves sometimes show significant differences from each other (41). Therefore, we have decided to take the alternative approach to analytically transform Eq. 1 and thus to take the slit-smearing effect into account. Because of the very narrow primary beam in the vertical direction, we have considered the horizontal-smearing effect only. For a primary beam with horizontal trapezium profile, and horizontal intensity distribution $W(x)$, as indicated in Fig. 3, the Eq. 1 is analytically transformed to

$$\tilde{I}(q) = \frac{1}{\xi^2(t - t_0)} \left(\frac{8A\pi\xi^2\left(t\,\text{ArcTan}\left[\frac{t\Xi}{\sqrt{q^2\Xi^2 + 1}}\right] - t_0\,\text{ArcTan}\left[\frac{t_0\Xi}{\sqrt{q^2\Xi^2 + 1}}\right]\right)\Xi^2}{(q^2\Xi^2 + 1)^{3/2}} + \right.$$

$$\left. + \frac{2B\xi\left(t\,\text{ArcTan}\left[\frac{t\xi}{\sqrt{q^2\xi^2 + 1}}\right] - t_0\,\text{ArcTan}\left[\frac{t_0\xi}{\sqrt{q^2\xi^2 + 1}}\right]\right)}{\sqrt{q^2\xi^2 + 1}} + B\left(\ln\left[(q^2 + t_0^2)\xi^2 + 1\right] - \ln\left[(q^2 + t^2)\xi^2 + 1\right]\right) \right). \quad (3)$$
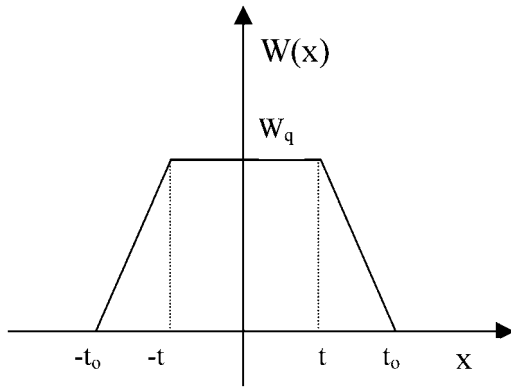
FIGURE 3 The horizontal intensity distribution $W(x)$ of a primary beam with horizontal trapezium profile as used in the experiment; x is the horizontal half-length of the beam, and t and t_o are absolute values of the scattering vectors at corresponding x. W_q is the trapezium height.

The term $\tilde{I}(q)$ denotes the smeared intensity. Here $A = W_q \Delta\rho^2 N \langle\delta\varphi^2\rangle$; N is the number of denser domains in the sample with average $\langle\delta\varphi^2\rangle$, and $B = W_q \Delta\rho^2 kT\varphi^2/M_{OS}$; x is the horizontal half-length of the beam; t and t_o are absolute values of the scattering vectors at corresponding x and are defined as $t = (2\pi/\lambda)(x/D)$, where D is the sample/detector distance. W_q is the trapezium height. Equation 3 is much too complex to be practicable. Assuming the trapezium profile to be equivalent to rectangular profile with a half-width of $w = (t + t_o)/2$, Eq. 3 reduces to

$$\tilde{I}(q) = 2\left(\frac{B\,\mathrm{ArcTan}\left[\frac{w\xi}{\sqrt{q^2\xi^2 + 1}}\right]}{\xi\sqrt{q^2\xi^2 + 1}} + 4A\pi\,\Xi^2\left(\frac{w\,\Xi}{(q^2\Xi^2 + 1)((w^2 + q^2)\Xi^2 + 1)} + \frac{\mathrm{ArcTan}\left[\frac{w\,\Xi}{\sqrt{q^2\Xi^2 + 1}}\right]}{(q^2\Xi^2 + 1)^{3/2}}\right)\right). \quad (4)$$

For infinite slit approximation, when w goes to infinity, Eq. 4 becomes simply

$$\tilde{I}(q) = \pi\left(\frac{B}{\xi\sqrt{q^2\xi^2 + 1}} + \frac{4A\pi\,\Xi^2}{(q^2\Xi^2 + 1)^{3/2}}\right). \quad (5)$$

We have fitted the experimental scattering curves with the above Eqs. 3–5 as given in Fig. 4. As one would expect, the best fits to the experimental data were obtained with Eq. 3. The use of the simpler Eq. 5 would be preferred; however, the quality of fits was unacceptable. On the other hand, assuming the trapezium profile to be equivalent to rectangular profile as given in Eq. 4 we have obtained adequate fits to the experimental data. Therefore, we have only used Eq. 4 in the subsequent data analyses.

The effect of pH on EPS scattering curves is shown in Fig. 5. The mathematical model gave satisfactory fits for all pH values. There was a pronounced increase in scattering intensity toward small q with a decrease in pH. Log-log plots at pH 10.5 indicated a linear relationship over more than one order-of-magnitude in q. With decreasing pH, the scattering curve bent and two approximately linear regions consistent with slopes a and b were apparent. Diversity of EPS structures at different pH values was even more pronounced on Kratky-Porod plots. For example, there was a broad peak at pH 10.5. With decreasing pH, the scattering intensity at low q increased and subsequently the broad peak disappeared. At low pH values there was a steep decrease in $I \times q$ intensity with increasing q followed by an approximately constant $I \times q$ region. As seen in Table 2, the static correlation length Ξ increased with lowering the pH and was positively correlated with parameter A^*, which embodies the product of the number of denser domains and the amplitudes of their mean-squared volume fraction fluctuations. The data also suggest that the dynamic correlation length ξ has a peak around pH $= 8.8$. A similar behavior was obtained for parameter B^*, which is a measure for osmotic susceptibility, φ^2/M_{OS}. Note also that although the calculated ionic strengths of various buffers are fairly high and different, they do not correlate with SAXS model parameters nor with the slopes. The model parameters and slopes, however, correlate with the proton concentration. The model gave the same ξ, Ξ, and A/B parameter values for either 0.4 or 1.0% concentration of the EPS in water (data not shown). This indicates that by increasing the concentration of the EPS macroscopic particles, the internal structure of the particles did not change.

DISCUSSION

In this work, structural properties of EPS isolated from a marine bacterium composed mainly of glucose have been studied at different pH and salt values by SAXS. The most intensive scattering of 0.4% (w/v) EPS solution occurred at small q-values, which suggests that large structures are present in the EPS. In addition, the presence of two nearly linear regions in the log-log scattering curves, with different slopes a and b, imply at least two SAXS size-scales in the EPS structure. Whereas slope a was clearly sensitive to pH,
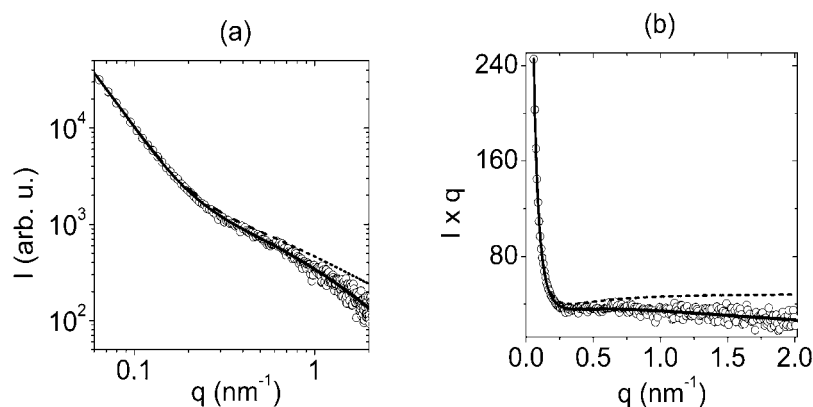
FIGURE 4   Experimental data (○) on log-log plots in *a* were fitted with Eq. 3 (——), Eq. 4 (. . .), and Eq. 5 (- - -). The same data are shown on a Kratky-Porod ($I \times q$ versus q) plot in *b* fitted with Eq. 3 (——), Eq. 4 (. . .), and Eq. 5 (- - -). In all three cases, the same values for parameters were used to produce the fit to the experimental data. The curve for Eq. 4 (. . .) cannot be seen, because it is nearly completely covered by the curve of Eq. 3 (——). In all subsequent analyses, we only used the simpler Eq. 4.

slope *b* was not. This further proposes that major structural rearrangements upon pH variation occur in EPS at larger SAXS spatial scale (i.e., low *q*). In contrast to pH, the addition of NaCl or $CaCl_2$ to 0.4% (w/v) EPS affected both slopes *a* and *b*. No change in slope *b* was observed with pH experiments alone, which suggests that the effect of ionic strength was less pronounced in pH experiments. To get a better understanding of the pH effect on EPS structure, we have used a modified version of the mathematical model proposed by Geissler et al. (36). The original model was transformed to take the slit-smearing effect into account. The refined mathematical model enabled us to fit the scattering curves of EPS from pH 0.7 to pH 11 satisfactorily. Although this does not by itself validate the model, it gives an estimate of structural rearrangement that is likely to take place in EPS with changing pH.

From the model it can be inferred that the EPS static correlation length Ξ, which in the literature is frequently interpreted as an average size of heterogeneous domains in polymeric networks, remained, at all values of pH, larger than dynamic correlation length, ξ, which is a measure for distances between polymeric chains in the network. This is, in general terms, consistent with results obtained by other researchers (34,38,39,42–45). For example, in 0.4% (w/v) EPS solutions we have found $\xi = 2$–5 nm, which is similar to the value found in carrageenan, $\xi = 3$–4 nm (34). However, the static correlation length, $\Xi = 15$–50 nm, was considerably different from that in carrageenan, $\Xi = 8$–10 nm.

At high pH, the EPS network appears to be structurally relatively homogenous. The number of denser domains, parameter *A*, as well as size of the denser domains Ξ, are the lowest. Data for different polymeric gels suggest that the dynamic correlation length ξ correlates well with osmotic susceptibility φ^2/M_{OS} (36–39), which is consistent with our observations. Both parameter *B* (a measure of osmotic susceptibility) and dynamic correlation length ξ reached the highest value around pH = 8.8. The increased ξ means that the average distance between chains increased, and this could be interpreted as swelling of the network. In general, at acidic pH, where EPS was less soluble, the ξ were smaller, while at alkaline pH the ξ were larger. In addition to swelling, the values for parameters *A* and Ξ increased as well. Since parameter *A* is proportional to the number of denser domains *N* and to the amplitude of polymer volume fraction fluctuations $\langle \delta\varphi^2 \rangle$, this indicates that either the number of denser domains or their density relative to that of the polymer network increased with decreased pH. In either case, the polymer network is less structurally homogenous at lower pH. Further decrease of pH from pH 8.8 to pH 0.7 caused the average distance between the polymer chains to decrease. Since this was accompanied by an increase in both the size of the denser domains and in parameter *A*, the EPS network is believed to de-swell. The model derived from these considerations is schematically depicted in Fig. 6.

The slope analysis of the scattering curves indicates the presence of two different size-scales in EPS. The decrease in slope *a* with decreased pH implies that larger EPS structures are becoming dominant at low pH. Based on the parameters in the mathematical model, this is consistent with an increase in the number and size of denser domains at low pH. Superimposed on this overall tendency of the EPS network to become less homogenous at low pH is swelling and de-swelling, as indicated by variations in the dynamic correlation length ξ and osmotic susceptibility *B*. On the other hand, slope *b* was, under all pH conditions, around -1. This corresponds to various fundamental models for scattering of coiled polymeric chains (45). Note that the scaling exponent for scattering from a random coil is -2, which transforms to -1 for infinite slit-smearing. The condensation of heterogeneous denser domains at low pH indicates that there might be pH-dependent charge effects present in the EPS structure. It is known from the solubility data on other polysaccharides that they are often soluble in alkaline solutions but insoluble at low pH (at room temperature) even when they do not contain charged groups (46). The chemical analysis revealed that, in addition to polysaccharides composed of uncharged glucose and galactose residues, EPS also contained ∼15% (w/w) proteins. In fact, the presence of proteins of various concentrations in EPS is common in the isolated EPS (3–6,15), as well as in native biofilms (47). The literature regarding
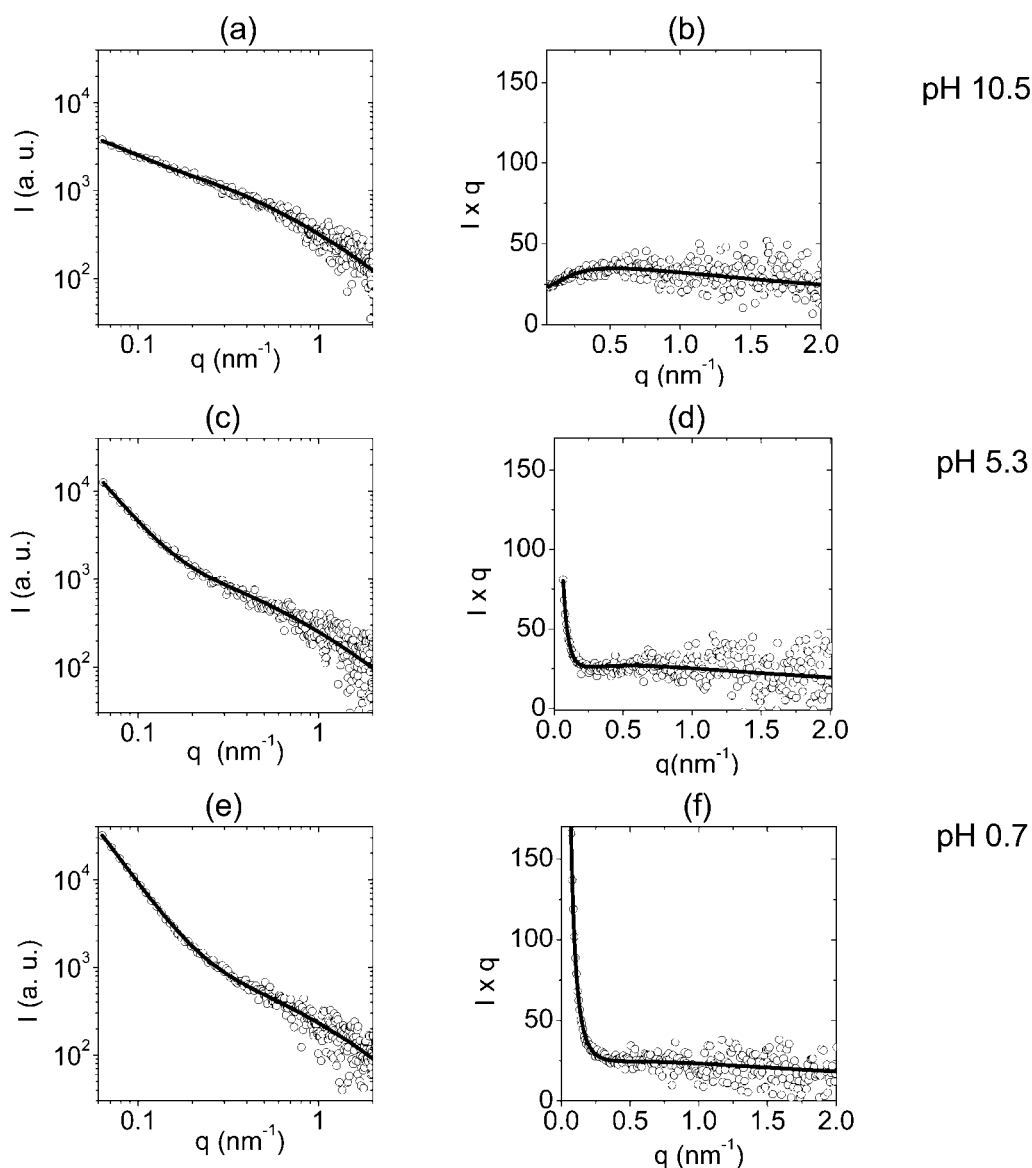
FIGURE 5 Log-log plots of scattering intensity of 0.4% EPS at different pH values are given in a, c, and e. Experimental data ($\bigcirc$), and best fits to the experimental data with Eq. 4 (—), are given. The same data are shown on a Kratky-Porod ($I \times q$ versus q) plot in b, d, and f. Both log-log and Kratky-Porod plots are given for three representative pH values. The parameters of the best fits are given in Table 2.

involvement of protein in the heterogeneous domain formation in polysaccharides is inconclusive. Tada et al. (48) reported that pure curdlan in 0.01 N NaOH forms networks with heterogeneous domains. SAXS studies of alginate gels also indicate formation of heterogeneous gels (40). Purified tamarind seed xyloglucan is believed to form local heterogeneities in 15% ethanol solutions (43). Anthonsen et al. (49) have also reported that purified chitosan forms aggregates and supramolecular structures. The treatment with proteinase, pH, and ionic-strength changes did not eliminate the aggregates. They claim that it was not possible to correlate the extent of aggregation with the chemical composition of chitosan. These studies would suggest that heterogeneous domains in poly-

saccharide matrices can also form in the absence of proteins. On the other hand, Mleko et al. (50) concluded from the SAXS curves that aggregates are formed in the mixture of whey proteins and carrageenan at acidic pH. They have also suggested that complexes between polysaccharides and proteins were formed. In the case of protein-nonionic hydrocolloid mixtures, pH only influences protein self-association. Nonionic hydrocolloid self-association, as well as protein-nonionic hydrocolloid cross-association, plays a minor role (51). Based on the discussion above, the proteins are not always necessary for heterogeneous domain formation in polysaccharides. However, due to their titratable groups, proteins may be involved in the observed pH structural response.

TABLE 2 Fitting parameters to SAXS data using Eq. 4 at different pH values

pH	$\Delta\rho^2/\Delta\rho^2_{max}$	$A^* \times 0.001$ (cm^{-4})	SD	Ξ (Å)	SD	$B^* \times 1000$ (cm^{-1})	SD	ξ (Å)	SD	R^2	I_s (M)
H$_2$O	1	98	0	379	2	10	0	25	0	0.999	≈ 0
11	1	2	0	190	50	7	1	36	5	0.907	1.15
10.5	0.94	6	1	150	20	28	3	42	3	0.988	1.14
8.8	0.82	35	1	230	10	46	4	48	3	0.997	1.72
7	0.36	49	1	280	20	28	2	28	2	0.988	1.36
5.3	0.74	52	1	330	20	18	2	33	2	0.996	0.66
2.5	0.74	116	2	360	10	7	1	26	3	0.999	1.74
0.7	0.78	166	4	520	20	8	1	23	1	0.997	0.4

I_s denotes calculated ionic strength of the solution.

SD is standard deviation for parameter.

*Indicates the multiplication of the parameter value by $\Delta\rho^2_{max}/\Delta\rho^2$. Note that A and B were also corrected for absorption.

The data in this study were obtained on an EPS isolated from a marine bacterium. The environmental pH of this marine EPS producer in the Adriatic Sea is from pH 8.10 to 8.25 and its salinity from 0.5 to 0.6 M. It is interesting to note that this is surprisingly close to the most swollen EPS structure observed in this study around pH 8.8. The data also indicate that EPS is a stable but flexible structure that is disrupted neither at pH 11 nor at pH 0.7. Since EPS is the first bacterial structure that comes into contact with the environment, its structural plasticity may enable bacteria to better respond to environmental stress.
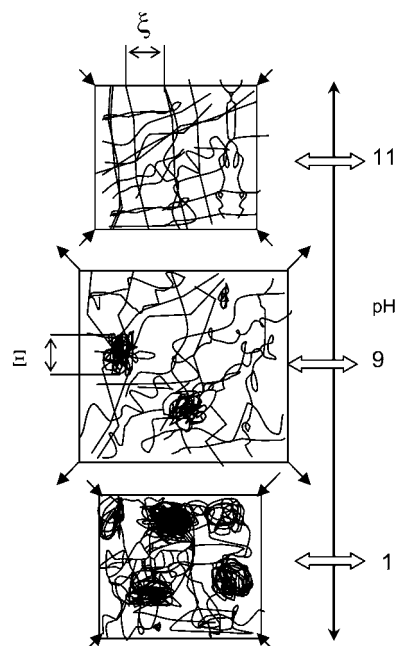

FIGURE 6 Schematic depiction of pH effect on EPS structure. Note that Ξ is an average size of denser domains in polymeric networks. Dynamic correlation length, ξ, is a measure of distances between polymeric chains in the network. At around pH = 11, the EPS structure is compact and homogenous. Denser domains occur at lower pH. The distance between polymeric chains, ξ, has a maximum around pH = 8.8, where the EPS structure is most swollen. With decreasing pH (i.e., at pH = 0.7), the EPS structure is composed of denser domains and is less homogenous.

CONCLUSIONS

The EPS isolated from a bacterial isolate from the Northern Adriatic Sea was composed mainly of glucose and a small fraction of galactose. The refined mathematical model presented here gives satisfactory fitting results for the EPS scattering curves in the range from pH 0.7 to pH 11.0. In terms of EPS structure, the SAXS data suggest that: 1), major structural rearrangements upon pH variations occur at large-size SAXS scales (i.e., between $d = 104.7$ nm and $d = 24.2$ nm); 2), ionic strength had an impact on EPS structure, but the effect was much smaller than the effect of pH; 3), on the small-size SAXS spatial scale, the effect of pH is not significant; and 4), upon pH decrease, the EPS that exists as a relatively homogeneous network at pH 11 swells up to pH 8.8, and with further decrease in pH, a less homogenous EPS network was observed.

REFERENCES

1. Sutherland, I. W. 1972. Bacterial exopolysaccharides. *Adv. Microb. Physiol.* 8:143–212.

2. Kumar, C. G., H. Joo, J. Choi, Y. Koo, and C. Chang. 2004. Purification and characterization of an extracellular polysaccharide from haloalkalophilic *Bacillus* sp. I-450. *Enzyme Microb. Technol.* 34: 673–681.

3. McKellar, R. C., J. van Geest, and W. Cui. 2003. Influence of culture and environmental conditions on the composition of exopolysaccharide produced by *Agrobacterium radiobacter*. *Food Hydrocolloids*. 17: 429–437.

4. Kachlany, S. C., S. B. Levery, J. S. Kim, B. L. Reuhs, L. W. Lion, and W. C. Ghiorse. 2001. Structure and carbohydrate analysis of the exopolysaccharide capsule of *Pseudomonas putida* G7. *Environ. Microbiol.* 3:774–784.

5. Beech, I., L. Hanjagsit, M. Kalaji, A. L. Neal, and V. Zinkevich. 1999. Chemical and structural characterization of exopolymers produced by *Pseudomonas* sp. NCIMB 2021 in continuous culture. *Microbiology.* 145:1491–1497.

6. Watanabe, M., Y. Suzuki, K. Sasaki, Y. Nakashimada, and N. Nishio. 1999. Flocculating property of extracellular polymeric substance derived from a marine photosynthetic bacterium, *Rhodovulum* sp. *J. Biosci. Bioeng.* 87:625–629.

7. Burdman, S., E. Jurkevitch, M. E. Soria-Díaz, A. M. Gil Serrano, and Y. Okon. 2000. Extracellular polysaccharide composition of *Azospirillum brasilense* and its relation with cell aggregation. *FEMS Microbiol. Lett.* 189:259–264.

8. Frank, B. P., and G. Belfort. 2003. Polysaccharides and sticky membrane surfaces: critical ionic effect. *J. Membr. Sci.* 212:205–212.

9. Joyce, J. G., C. Abeygunawardana, Q. Xu, J. C. Cook, R. Hepler, C. T. Przysiecki, K. M. Grimm, K. Roper, C. C. Yu, L. Ip, D. Cope, M. Montgomery, S. Chang, M. Campie, T. B. Brown, J. McNeely, T. Zorman, G. B. Maria-Litrán, P. Pier, M. Keller, K. U. Jansen, and G. E. Mark III. 2003. Isolation, structural characterization, and immunological evaluation of high-molecular-weight weight exopolysaccharide from *Staphylococcus aureus*. *Carbohydr. Res.* 338:903–922.

10. Cescutti, P., R. Toffanin, P. Pollesello, and I. W. Sutherland. 1999. Structural determination of the acidic exopolysaccharide produced by a *Pseudomonas* sp. strain 1.15. *Carbohydr. Res.* 315:159–168.

11. Decho, A. W. 2000. Microbial biofilms in an intertidal system: an overview. *Cont. Shelf Res.* 20:1257–1273.

12. Looijesteijn, P. J., L. Trapet, E. de Vries, T. Abbe, and J. Hugenholtz. 2001. Physiological function of exopolysaccharides produced by *Lactococcus lactis*. *Int. J. Food Microbiol.* 64:71–80.

13. De Vuyst, L., and B. Degeest. 1999. Heteropolysaccharides from lactic acid bacteria. *FEMS Microbiol. Rev.* 2:153–177.

14. Faber, E. J., J. P. Kamerling, and J. F. G. Vliegenhart. 2001a. Structure of the extracellular polysaccharides produced by *Lactobacillus delbrueckii* ssp. *Bulgaricus* 291. *Carbohydr. Res.* 331:183–194.

15. Kumar, C. G., and S. K. Anand. 1998. Significance of microbial biofilms in food industry: a review. *Int. J. Food Microbiol.* 42:9–27.

16. Stephens, C. 2002. Microbiology: breaking down biofilms. *Curr. Biol.* 12:132–134.

17. Characklis, W. G. 1990. Microbial fouling. *In* Biofilms. W.G. Characklis and K.C. Marshall, editors. Wiley Press, New York. 523–584.

18. Little, B. J., P. A. Wagner, W. G. Characklis, and K. C. Marshall. 1990. Microbial corrosion. *In* Biofilms. W.G. Characklis and K.C. Marshall, editors. Wiley Press, New York. 635–670.

19. Gamini, A., S. Paoletti, R. Toffanin, F. Micali, L. Michielin, and C. Bevilacqua. 2002. Structural investigations of cross-linked hyaluronan. *Biomaterials.* 23:1161–1167.

20. Yun, U. J., and H. D. Park. 2003. Physical properties of an extracellular polysaccharide produced by *Bacillus* sp. CP912. *Lett. Appl. Microbiol.* 36:282–287.

21. Villain-Simonnet, A., M. Milas, and M. Rinaudo. 1999. Comparison between the physicochemical behaviour of the two microbial polysaccharides: RMDP17 and rhamsan. *Int. J. Biol. Macromol.* 26:55–62.

22. Ridout, M. J., G. J. Brownsey, A. P. Gunning, and V. J. Morris. 1998. Characterisation of the polysaccharide produced by *Acetobacter xylinum* strain CR1/4 by light scattering and atomic force microscopy. *Int. J. Biol. Macromol.* 23:287–293.

23. Ding, Q., M. LaBelle, B. Y. Yang, and R. Montgomery. 2003. Physicochemical studies of extracellular polysaccharides of *Erwinia chrysanthemi* spp. *Carbohydr. Polym.* 51:333–346.

24. Hirata, Y., Y. Sano, M. Aoki, H. Shohji, S. Katoh, J. Abe, S. Hitsukuri, and H. Yamamoto. 2003. Small angle x-ray scattering studies of moderately concentrated dextran solution. *Carbohydr. Polym.* 53:331–335.

25. Yuguchi, Y., H. Urakawa, and K. Kajiwara. 2002. The effect of potassium salt on the structural characteristics of gellan gum gel. *Food Hydrocolloids.* 16:191–195.

26. Yuguchi, Y., H. Urakawa, and K. Kajiwara. 2003. Structural characteristics of carrageenan gels: various types of counter ions. *Food Hydrocolloids.* 17:481–485.

27. Mischenko, N., B. Denef, M. H. J. Koch, and H. Reynaers. 1996. Influence of ionic effects on the ordering and association phenomena in dilute and semidilute carrageenan solutions. *Int. J. Biol. Macromol.* 19:185–194.

28. Yang, Z., E. Huttunen, M. Staaf, G. Widmalm, and H. Tenchu. 1999. Separation, purification and characterization of extracellular polysaccharides produced by slime-forming *Lactococcus lactis* ssp. *cremoris* strains. *Int. Dairy J.* 9:631–638.

29. Tada, T., T. Matsumoto, and T. Masuda. 1998. Structure of molecular association of curdlan at dilute regime in alkaline aqueous systems. *Chem. Phys.* 228:157–166.

30. Faber, E. J., M. J. van den Haak, J. P. Kamerling, and J. F. G. Vliegenhart. 2001b. Structure of the exopolysaccharide produced by *Streptococcus thermophilus* S3. *Carbohydr. Res.* 331:173–182.

31. Pukl, M., and M. Prosek. 1990. Rapid quantitative TLC analysis of sugars using an improved commonly used solvent system. *J. Planar Chromatogr.* 3:173–176.

32. Laggner, P., and H. Mio. 1992. SWAX: a dual-detector camera for simultaneous small- and wide-angle x-ray diffraction in polymer and liquid crystal research. *Nucl. Instrum. Methods Phys. Res. A.* 323:86–90.

33. Munter, A. 2003. Scattering length density calculator. National Institute of Standards and Technology, Center for Neutron Research, Gaithersburg, MD. Http://www.ncnr.nist.gov/resources/sldcalc.html.

34. Evmenenko, G., E. Theunissen, K. Mortensen, and H. Reynaers. 2001. SANS study of surfactant ordering in κ-carrageenan/cetylpyridinium chloride complexes. *Polymers.* 42:2907–2913.

35. Trpinac, P. 1965. Chemistry Practicum for Medicine and Stomatology Students, 6th Ed., Teaching Book, Belgrade, Yugoslavia.

36. Geissler, E., F. Horkay, A. Hecht, C. Rochas, P. Linder, C. Bourgaux, and G. Courraze. 1997. Investigation on PDMS gels and solutions by small angle scattering. *Polym.* 36:15–20.

37. Horkay, F., A. M. Hecht, M. Zrínyi, and E. Geissler. 1996. Effect of cross-links on the structure of polymer gels. *Polym. Gel. Net.* 4:451–465.

38. Horkay, F., G. B. McKenna, P. Deschamps, and E. Geissler. 2000. Neutron scattering properties of randomly cross-linked polyisoprene gels. *Macromolecules.* 33:5215–5220.

39. Hecht, A. M., F. Horkay, and E. Geissler. 2001. Neutron scattering investigation on a bimodal polymer gel. *J. Phys. Chem.* 105:5637–5642.

40. Draget, I. K., B. T. Stokke, Y. Yuguchi, H. Urakawa, and K. Kajiwara. 2003. Small-angle x-ray scattering and rheological characterization of alginate gels. III. Alginic acid gels. *Biomacromolecules.* 4:1661–1668.

41. Roe, R. J. 2000. Methods of X-Ray and Neutron Scattering in Polymer Science. Oxford University Press, New York.

42. Evmenenko, G., and T. Budtova. 2000. Structural changes in hydrogels immersed in a linear polymer solution, studied by SANS. *Polymers.* 41:4943–4947.

43. Yamanaka, S., Y. Yuguchi, H. Urakawa, K. Kajiwara, M. Shirakawa, and K. Yamatoya. 2000. Gelation of tamarind seed polysaccharide xyloglucan in the presence of ethanol. *Food Hydrocolloids.* 14:125–128.

44. Milimouk, I., A. M. Hecht, D. Beysens, and E. Geissler. 2001. Swelling of neutralized polyelectrolyte gels. *Polymers.* 42:487–494.

45. Daoud, M., and J. E. Martin. 1989. Fractal properties of polymers. *In* The Fractal Approach to Heterogeneous Chemistry. D. Avnir, editor. John Wiley & Sons Ltd., New York. 109–129.

46. Rauen, H. M. 1964. Biochemistry Handbook, 2nd Ed. Springer-Verlag, Heidelberg, Germany.

47. Sutherland, I. W. 2001. Biofilm exopolysaccharides: a strong and sticky framework. *Microbiol.* 147:3–9.

48. Tada, T., T. Matsumoto, and T. Masuda. 1999. Dynamic viscoelasticity and small-angle x-ray scattering studies on the gelation mechanism and network structure of curdlan gels. *Carbohydr. Polym.* 39:53–59.

49. Anthonsen, M. W., K. M. Vårum, A. M. Hermansson, O. Smidsrød, and D. A. Brant. 1994. Aggregates in acidic solutions of chitosans detected by static laser light scattering. *Carbohydr. Polym.* 25:13–23.

50. Mleko, S., E. C. Y. Li-Chan, and S. Pikus. 1997. Interactions of κ-carrageenan with whey proteins in gels formed different pH. *Food Res. Int.* 30:427–433.

51. Syrbe, A., W. J. Bauer, and H. Klostermeyer. 1998. Polymer science concepts in dairy systems—an overview of milk protein and food hydrocolloid interaction. *Int. Dairy J.* 8:179–193.